El Niño-Southern Oscillation Complexity

Axel Timmermann[1,2], Soon-Il An[3], Jong-Seong Kug[4], Fei-Fei Jin[5], Wenju Cai[6], Antonietta Capotondi[7,8], Kim Cobb[9], Matthieu Lengaigne[10], Michael J. McPhaden[11], Malte F., Stuecker[12,13], Karl Stein[1], Andrew T. Wittenberg[14], Kyung-Sook Yun[1], Tobias Bayr[15], Han-Ching Chen[16], Yoshimitsu Chikamoto[17], Boris Dewitte[18], Dietmar Dommenget[19], Pamela Grothe[20], Eric Guilyardi[21,22], Yoo-Geun Ham[23], Michiya Hayashi[5], Sarah Ineson[24], Daehyun Kang[25], Sunyong Kim[4], WonMoo Kim[26], June-Yi Lee[1], Tim Li[2,5], Jing-Jia Luo[27], Shayne McGregor[19], Yann Planton[21], Scott Power[27], Harun Rashid[6], Hong-Li Ren[28], Agus Santoso[29], Ken Takahashi[30], Alexander Todd[31], Guomin Wang[27], Guojian Wang[6], Ruihuang Xie[32], Woo-Hyun Yang[4], Sang-Wook Yeh[33], Jinho Yoon[34], Elke Zeller[1], Xuebin Zhang[35]

[1] Center for Climate Physics, Institute for Basic Science (IBS), Pusan National University, Busan, Republic of Korea
[2] International Pacific Research Center, University of Hawaii at Manoa, Honolulu, Hawaii, USA.
[3] Department of Atmospheric Sciences, Yonsei University, Seoul, Korea
[4] Division of Environmental Science & Engineering, Pohang University of Science and Technology (POSTECH), Pohang 37673, South Korea
[5] Department of Atmospheric Science, SOEST, University of Hawaii at Manoa, Honolulu, Hawaii, USA
[6] CSIRO Oceans and Atmosphere, Aspendale, Victoria 3195, Australia
[7] Cooperative Institute for Research in Environmental Science, University of Colorado, Boulder CO, 80309, USA
[8] Physical Sciences Division, NOAA Earth System Research Laboratory, Boulder CO, 80305, USA
[9] Earth & Atmospheric Sciences, Georgia Tech, MC 0340 311 Ferst Drive Atlanta, USA
[10] Sorbonne Universités (UPMC, Univ. Paris 06) CNRS-IRD-MNHN, LOCEAN laboratory, IPSL, Paris, France
[11] Pacific Marine Environmental Laboratory/NOAA, Seattle Washington, USA
[12] Department of Atmospheric Sciences, University of Washington, Seattle, Washington, USA
[13] Cooperative Programs for the Advancement of Earth System Science, University Corporation for Atmospheric Research, Boulder, Colorado, USA
[14] Geophysical Fluid Dynamics Laboratory/NOAA, Princeton, New Jersey 08540-6649, USA.
[15] GEOMAR Helmholtz Centre for Ocean Research Duesternbrooker Weg 20, 24105 Kiel, Germany
[16] Department of Atmospheric Sciences, National Taiwan University, Taipei, Taiwan
[17] Department of Plants, Soils, and Climate, Utah State University, Utah, USA
[18] Centro de Estudios Avanzado en Zonas Áridas (CEAZA), Coquimbo, Chile. & Laboratoire d'Etudes en Géophysique et Océanographie Spatiale, Toulouse, France
[19] School of Earth, Atmosphere and Environment, Monash University, Clayton, Australia
[20] Department of Earth and Environmental Sciences, University of Mary Washington, Fredericksburg, VA, USA
[21] Laboratoire d'Océanographie et du Climat: Expérimentation et Approches Numériques (LOCEAN), IRD/UPMC/CNRS/MNHN, Paris Cedex 05, France.
[22] NCAS-Climate, University of Reading, Reading RG6 6BB, UK
[23] Department of Oceanography, Chonnam National University, Gwangju, South Korea
[24] Met Office Hadley Centre, FitzRoy Road, Exeter, EX1 3PB, U.K.
[25] School of Urban and Environmental Engineering, Ulsan National Institute of Science and Technology, 44919, Ulsan, South Korea.

42   26Climate Prediction Department, APEC Climate Center, Busan, Korea,

43   27Australian Bureau of Meteorology, Melbourne, Australia

44   28Laboratory for Climate Studies, National Climate Center, China Meteorological Administration, Beijing, China

45   29ARC Centre of Excellence for Climate System Science, Faculty of Science, University of New South Wales, Sydney,

46   NSW 2052, AUSTRALIA

47   30Instituto Geofisico del Peru, Lima, Peru

48   31University of Exeter College of Engineering, Mathematics and Physical Sciences, Exeter, UK

49   32Institute of Oceanology, Chinese Academy of Sciences, Qingdao, P. R. China

50   33Department of Marine Sciences and Convergent Technology, Hanyang University, Ansan, South Korea

51   34School of Earth Sciences and Environmental Engineering, Gwangju Institute of Science and Technology, Gwangju,

52   61005, South Korea

53   35CSIRO Ocean and Atmosphere, Hobart TAS 7001, Australia

54   *Correspondence to: Axel Timmermann. IBS Center for Climate Physics, Pusan National University,

55   Busan, Republic of Korea (E-mail: timmermann@pusan.ac.kr).

56

57   **El Niño events are characterized by tropical Pacific surface warming and weakening of**

58   **trade winds occurring every few years. Such conditions are accompanied by changes in**

59   **atmospheric and oceanic circulation, affecting global climate, marine and terrestrial**

60   **ecosystems, fisheries and human activities. The alternation of warm El Niño and cold La**

61   **Niña conditions, referred to as the El Niño-Southern Oscillation (ENSO), represents the**

62   **strongest year-to-year fluctuation of the global climate system. Here we provide a**

63   **synthesis of our current understanding of the spatio-temporal complexity of this**

64   **important climate mode and its influence on the earth system.**

65

66   ## 1) Introduction

67   Originally described in 1893 as "corriente del Niño"[1] – a warm regional ocean current

68   that affected regional climate off the coast of Peru – the view on the El Niño

69   phenomenon has changed over the past century. In the 1960s ENSO was recognized as a

70   basin-scale phenomenon involving coupled atmosphere-ocean processes[2]. A major

71   international research program in the 1980s and 90s fundamentally advanced the

72   ability to observe, understand and predict ENSO and its world-wide impacts[3]. During

73   the past 20 years the understanding has continued to evolve as new layers of

74   complexity (Box 1) were identified in ENSO dynamics and predictability. The concept of

75   El Niño has developed from one of a canonical progression of phases from onset,

76   maturity and demise[4] (Figure 1) to one that accounts for its spatio-temporal complexity

77   (Figure 2) and varying climatic impacts[5-8] (Figure 3). We have also come to realize that

78   although ENSO primarily manifests itself as a year-to-year climate fluctuation, its
79   dynamics involves a broad range of processes interacting on timescales from weeks[9,10]
80   to decades[11,12]. This complexity introduces new challenges for seasonal forecasting.
81
82   The most recent El Niño[13] in 2015/16 was initiated in boreal spring by a series of
83   Westerly Wind Events (WWE) (Box 1, Figure 3e) – a form of weather noise. The
84   associated wind forcing triggered downwelling oceanic Kelvin waves (Box 1, Figure 1),
85   reducing the upwelling of cold subsurface waters in the Eastern Pacific Cold Tongue
86   (Box 1) and leading to a central and eastern Pacific surface warming. The positive Sea
87   Surface Temperature Anomaly (SSTA) shifted atmospheric convection from the
88   Western Pacific Warm Pool (Box 1) to the central equatorial Pacific, causing a reduction
89   in equatorial trade winds, which in turn intensified surface warming through the
90   positive Bjerknes feedback (Box 1). The seasonally-paced termination of the 2015/16
91   event (Figure 3e) was associated with ocean dynamics and the slow discharge of
92   equatorial heat into off-equatorial regions thus providing a delayed negative feedback
93   (Box 1). The event started to decline in early 2016 and transitioned into a weak La Niña
94   in mid 2016.
95
96   In broad terms this evolution is common to the other strong El Niño events in 1982/83
97   and 1997/98 (Figure 3c). However, no two events are alike – be they strong, moderate
98   or weak (Figure 2, 3 f-m). This diversity arises from the varying roles of noise forcing
99   (Figure 3c-e) and of positive and negative coupled atmosphere/ocean feedback
100   processes[14] (Box 1) that act to enhance and suppress growth of SST anomalies,
101   respectively. The complexity of ENSO patterns, amplitude and temporal evolution –
102   referred to as ENSO Complexity (Box 1) – along with internal atmospheric noise may
103   also translate into a diversity of global impacts[7,15]. When the underlying SSTs change in
104   the equatorial Pacific, there are shifts in atmospheric deep convection, which in turn
105   cause adjustments of the global Walker Circulation (Box 1) and generate stationary
106   atmospheric waves[16] that impact the far reaches of our planet. This perturbed global
107   circulation influences weather variability leading to massive reorganizations of global
108   temperature and rainfall patterns[17,18] (Figure 3f-m).
109
110   Paleo-climate reconstructions of the ENSO phenomenon across the mid-late Holocene[19]

111   also show a wide range of amplitudes, thus highlighting the importance of internal
112   climate processes in modulating ENSO's complexity on timescales ranging from decades
113   to centuries. In addition, the activity of reconstructed ENSO variability shows an
114   intensification in the late 20th Century relative to other pre-industrial periods[19,20], thus
115   raising the general question of whether external forcings could influence ENSO's
116   evolution and amplitude. How ENSO responds to greenhouse warming is one of the
117   most compelling outstanding questions[21].

118

119   Given the societal and environmental relevance of ENSO, it is paramount to improve our
120   understanding of the processes that control ENSO's amplitude, timing, duration,
121   predictability and global impacts. Here we synthesize our current understanding of
122   ENSO dynamical processes and their role in controlling ENSO complexity. Against this
123   backdrop we will highlight areas of uncertainty (section 6) as a stimulus for further
124   research.

125

126   ## 2) A conceptual view of ENSO dynamics

127   Early efforts to elucidate the dynamics of ENSO focused on the average (composite)
128   evolution of El Niño events[22], capturing the typical evolution of ocean and atmosphere
129   conditions from early spring initiation of El Niño to a wintertime peak and transition to
130   La Niña during the subsequent summer (Figure 1). The enhanced spectral interannual
131   variability of ENSO (Figure 3a,b) has been explained by invoking positive
132   atmosphere/ocean feedbacks and delayed negative ocean adjustment feedbacks (Box
133   1), which together can lead to oscillatory dynamics, as encapsulated by the delayed
134   action oscillator[23] and recharge oscillator[24] modelling frameworks. In its most general
135   form, the ENSO recharge oscillator model can be expressed as:

136

$$\frac{dT_e}{dt} = I_{BJ}T_e + Fh$$
$$\frac{dh}{dt} = -\varepsilon h - \alpha T_e,$$

140

141   [equation (1)] where T_e and h represent the equatorial eastern Pacific surface
142   temperature and zonal mean thermocline depth, respectively. The Bjerknes stability
143   index I_{BJ} (referred to as the BJ index or ENSO linear growth rate; Figure 1j) depends on a

144 number of processes such as thermocline-, zonal advective- and Ekman-feedbacks to

145 reinforce SST, and thermal advection by horizontal mean surface currents and thermal

146 damping by net surface heat fluxes as negative feedbacks[14] (Box 1). In equation (1) ε

147 represents a damping rate of thermocline depth anomalies. The interannual timescale

148 of the ENSO system is mainly determined by F and α, which capture the thermocline

149 feedback (Box 1) and the slow equatorial recharge/discharge process (Box 1)

150 associated with the oceanic heat transport, respectively. For constant I_{BJ} the model

151 describes a linear recharge oscillator: Starting from neutral conditions $T_e{\sim}0$ (typically

152 in boreal winter-spring, Figure 1c, 2) and a charged thermocline state $h>0$, an El Niño

153 can grow (Figure 1d,e, 2). While eastern equatorial Pacific SSTA develop, the

154 thermocline feedback (Box 1) Fh further intensifies the growth of SSTA by upwelling

155 anomalously warm subsurface waters to the surface in the Eastern Pacific Cold Tongue.

156 Moreover, positive eastern Pacific SSTA $(T_e>0)$ cause a weakening of the equatorial

157 trade winds (Figure 1d,e). The associated wind-stress curl discharges the equatorial

158 heat through Sverdrup transport (Box 1) and ocean boundary processes (Figure 1f).

159 The resulting drainage of heat in turn weakens the thermocline feedback, and the ENSO

160 recharge oscillator can transition into a La Niña state (Figure 1g,h), which is

161 accompanied by a recharging of heat through opposite wind-stress curl anomalies

162 (Figure 1h).

163

164 Comparing the linear oscillator solution of equation (1) ($I_{BJ}=const$) with the scatterplot

165 of observed equatorial eastern Pacific temperature and zonal mean thermocline depth

166 anomalies (Figure 2), we find substantial differences. The observed scatter diagram

167 shows a high degree of irregularity and a notable positive skewness in eastern tropical

168 Pacific SSTA towards El Niño events (Box 1, Figure 2). El Niño and La Niña events are

169 very different in terms of their amplitude and time-evolution (Figure 1k, 2a). To

170 account for this additional level of complexity the simple recharge oscillator model can

171 be extended by including a nonlinear Bjerknes feedback term that represents either

172 atmospheric or oceanic nonlinear processes[25] or multiplicative stochastic forcing[26] (Box

173 1). For these extensions, the recharge model can then simulate ENSO's skewed

174 probability distribution (Figure 2) and the fast growth from neutral to strong El Niño

175 conditions (Figure 1j). The observed positive skewness of SSTA (Figure 2), which

176 indicates the importance of nonlinear dynamical and thermodynamical processes in the

177   coupled tropical Pacific climate system, implies that strong El Niño conditions, which

178   typically last for 1 year, are on average shorter than La Niña events, which can persist

179   for up to several years (Figure 1k).

180

181   Whereas conceptual models like equation (1) can simulate some key features of ENSO's

182   evolution, they can neither explain the presence of ENSO's spatial diversity (Figure

183   3a,b,f-m), nor the potential remote effects of variability originating from the extra-

184   tropical Pacific, Atlantic or Indian Ocean onto this diversity. An improved framework to

185   characterize and explain ENSO complexity is needed to capture these aspects.

186

187   **3) Space-time complexity of ENSO**

188   In spite of some prominent commonalities discussed in section 2 (Figure 1), El Niño

189   events differ considerably from each other in terms of magnitude, spatial pattern,

190   temporal evolution, and predictability[5-7,27] (Figure 2, 3 f-m). To characterize the leading

191   modes of equatorial Pacific SST variability, and their diverse timescales, we conduct an

192   Empirical Orthogonal Function (EOF) analysis of observed tropical Pacific SSTA[28]

193   (Figure 3), which identifies the leading orthogonal patterns of variability. The leading

194   EOF (Figure 3a), which corresponds to the classical El Niño pattern with eastern

195   tropical Pacific warming, exhibits variability on quasi-quadrennial time scales (3-7

196   years) (spectral density estimate in Figure 3a). In contrast, the second EOF, which

197   explains only 25% of the variance of the first mode, is characterized by an east/west

198   zonal SST dipole in the tropical Pacific and has enhanced variance on quasi-biennial and

199   decadal timescales (spectral density estimate Figure 3b). The interplay of these two

200   EOFs largely captures the spatial diversity of the observed ENSO mode.

201

202   Some El Niño events (e.g. 1997/98) (Figure 3c,f) are characterized by pronounced

203   warming in the Eastern Pacific (referred to as EP El Niño events), while others show a

204   stronger positive projection on the second EOF mode, which leads to a more

205   pronounced Central Pacific warming (referred to as CP El Niño events) (e.g. 2004/05)

206   (Figure 3d,h,i,j). More generally, El Niño events can be viewed as the superposition of

207   the two EOF modes, resulting in a continuum of ENSO flavors[29,30] that capture a mix of

208   EP and CP dynamics (e.g. 1991/92 and 2016/17 events) (Figure 2). La Niña events (e.g.

209   1999/2000) (Figure 3g), in addition to being weaker, exhibit less diversity in their

210 spatial patterns[6,31], thus clearly pointing to an asymmetry in the underlying dynamical
211 processes for ENSO.

212

213 EP El Niño events (e.g. 1997/98) (Figure 3c) tend to involve basin-scale equatorial wind
214 anomalies, a strong relaxation of the zonal tilt of the equatorial thermocline (Figure 1e),
215 a more prominent role for the thermocline feedback (Box 1), large eastward shifts of
216 tropical Pacific convection, and strong discharge of heat content (Figure 3c) from the
217 equatorial region, which boosts the likelihood of transitioning into a La Niña event[6,27].
218 In contrast, CP El Niño events (e.g. 2004/05) (Figure 3d) tend to involve more local
219 wind feedbacks, a stronger role for the zonal advective feedback (Box 1), little reduction
220 in the zonal tilt of the thermocline, weak shifts of convection, earlier termination, little
221 poleward discharge of ocean heat content (Figure 3d), a stronger role for thermal
222 damping (Box 1) during the decay phase, a reduced likelihood to transition into La Niña,
223 and more susceptibility to disruption by wind noise[6,27]. Compared to CP El Niños,
224 strong EP El Niños also tend to terminate later in boreal spring, due to a trade wind
225 collapse which suppresses the upwelling that normally connects the SST to the evolving
226 thermocline depth[32].

227

228 The spatial diversity in ENSO's SSTA patterns is also associated with different tropical
229 precipitation patterns (Figure 3f-m), resulting in potentially different remote
230 teleconnection patterns and corresponding weather and climate impacts[7,33]. However,
231 the length of the historical record is not sufficient to permit robust detection of
232 differences in the impacts of the various El Niño flavors, given the high level of internal
233 atmospheric variability[34]. In addition to its spatial diversity, ENSO also exhibits
234 substantial diversity in its temporal evolution (Figure 1k, 3 c,d,e).

235

236 Understanding this diversity of El Niño events is crucial for predicting ENSO's regional
237 impacts, e.g. on precipitation patterns, tropical cyclones, and other severe weather[5]. The
238 extent to which El Niño diversity is predictable relates to whether ENSO's complexity
239 originates mainly from random processes, or from low-frequency deterministic
240 dynamics. Random processes affecting a single physical ENSO mode could generate
241 diversity in amplitude, spatial structure, and temporal evolution[8], consistent with a
242 spatial flavor continuum generated by different realizations of atmospheric noise[29].

243 Alternatively, initial subsurface ocean conditions could modulate the role of stochastic
244 wind forcing in producing diversity. For example, climate model simulations have
245 demonstrated that in the presence of stochastic WWEs, an initial buildup of equatorial
246 Pacific upper-ocean heat content can favor the development of EP rather than CP El
247 Niño events[10,35,36] (Figure 3d,e). At the onset of strong El Niño events[37] such as 1997/98
248 and 2015/16 (Figure 3c,e), WWE activity tends to strengthen and expand eastward
249 with the expansion of the Western Pacific Warm Pool and the relaxation of the trade
250 winds. These WWE changes can be parameterized in equation (1) as multiplicative
251 noise (Box 1), which can contribute to ENSO diversity and asymmetries[9,38].

253 Studies suggest that ENSO diversity may be triggered by climate phenomena outside the
254 tropical Pacific, including the North[39] and South Pacific[40] meridional modes, extra-
255 tropical atmospheric circulation patterns, and tropical Atlantic variability[5,41,42]. For
256 example, the negative phase of the North Pacific Oscillation[43] tends to favor the
257 development of positive SST anomalies in the central Pacific by weakening the trade
258 winds in the northern Hemisphere, while the positive phase of the South Pacific
259 Oscillation tends to weaken the southern Hemisphere trades and favor the development
260 of positive SSTAs in the eastern Pacific. Such remote influences appear to be mediated
261 primarily by how they project onto wind variations in the equatorial Pacific. In essence,
262 westerly wind anomalies in the western equatorial Pacific tend to favor CP El Niños,
263 while westerly wind anomalies in the central-eastern equatorial Pacific tend to favor EP
264 El Niños. These external influences can precede the peak of El Niño by 2-3 seasons[41,43]
265 and may provide additional predictability to the spatial characteristics of an emerging
266 El Niño event.

268 Since 1998, CP events have been more prevalent than EP events[44]. Such a decadal
269 modulation in ENSO diversity is consistent with CGCMs that can spontaneously
270 generate multidecadal variations in ENSO diversity even in the absence of external
271 radiative forcings[45]. Low-frequency climatic drivers (including natural and
272 anthropogenic forcings) — which involve basinwide changes in the zonal SST gradient,
273 thermocline depth, and winds[46,47] — may also have contributed to the observed decadal
274 swings in ENSO diversity by favoring particular spatio-temporal modes[48]. At this stage,

275   the observational record remains too short to quantify all the possible sources of the
276   decadal modulation of ENSO characteristics.

277

278   The current generation of climate models underestimates ENSO diversity[49]. This issue is
279   related to the models' systematic biases, which affect the mean state and ENSO
280   feedbacks. Sources of these biases include deficiencies in the simulation of clouds,
281   atmospheric convection, and oceanic mixing[50]. In particular, atmospheric model
282   responses tend to be relatively insensitive to distinct patterns of SST anomalies, due to
283   climatological dry and cold biases in the equatorial central Pacific[49,51].

284

285   **4) Seasonal ENSO dynamics**
286   ENSO displays a close relationship with the seasonal cycle[22,52]: El Niño events usually
287   start in boreal spring (Figure 1c,i, 4), grow during the summer and fall (Figure 1d),
288   reach their maximum intensity in winter (Figure 1e,i), and decay rapidly during late
289   winter and spring (Figure 1f,j). In most cases, by the subsequent summer, they
290   transition to La Niña events (Figure 1g,h, 4). This seasonal synchronization of ENSO
291   translates into the observed eastern equatorial Pacific SSTA variance peaking during
292   boreal winter and attaining minimum values during spring (Figure 1j). It also leads to
293   pronounced seasonal contrasts in ENSO's climate impacts and predictability (Figure 1i).
294   ENSO influences the global atmospheric circulation, affecting the Asian Monsoons[53],
295   America[54], and Australia[55].

296

297   Randomly occurring sequences of WWEs, typically during spring, can lead to an initial
298   warming of the central-eastern equatorial Pacific[56] (Figure 1c). This initial SSTA can
299   grow because the air-sea coupling is strongest in summer and early fall[57,58] (Figure 1j).
300   Proposed physical processes for this summer/fall coupling maximum include (i) the
301   equatorward shift of the ITCZ[59] and its associated increase in western Pacific surface
302   wind convergence[59], (ii) the seasonal outcropping of the equatorial thermocline[60], (iii)
303   the seasonal cooling of the eastern equatorial Pacific[59], (iv) and the reduction of the
304   negative cloud feedbacks[61].

305

306   The decay of El Niño events typically starts in boreal winter. The anomalous westerlies
307   shift southward from the equator, leading to a shoaling of the eastern Pacific

thermocline, and a subsequent reduction of the overlying SSTA[62] (Figure 1f, 4a). This shift arises from climatological expansion of the Western Pacific Warm Pool into the Southern Hemisphere, coincident with the development of the South Pacific Convergence Zone[63]. In this season, the increased surface heat flux damping[61] results in a decrease of the air-sea coupling strength (Figure 1j), which together with the aforementioned seasonal southward wind shift[64] and the equatorial heat content discharge[24] (Figure 4b) lead to a rapid transition to a La Niña state.

While these seasonal processes generally operate for different flavors and phases of ENSO, differences in their relative importance can contribute to ENSO complexity. For instance, CP events typically terminate earlier and are less likely to transition to a La Niña state compared to EP El Niño events[63] (Figure 3d). Furthermore, La Niña conditions can last up to 2-3 years (Figure 3c, 4b). The ability to simulate ENSO seasonal synchronization for different types of El Niño events varies strongly among the current generation of climate models, likely due to biases in mean state and seasonal cycle[57].

The influence of the seasonal variations of the air-sea coupling strength discussed above can be included in the framework of the recharge oscillator [equation (1)] by adding a seasonally varying growth rate (I_{BJ}). As expected, this model captures the observed ENSO seasonal synchronization characteristics, including the seasonal ENSO variance modulation and partial phase synchronization[25]. Interactions between the seasonal cycle in I_{BJ} and the interannual ENSO temperature signal generate variance with periods at roughly 9 and 15-18 months, the so-called combination tone frequencies (Box 1) that broaden the ENSO spectrum predominantly towards higher frequencies[65,66]. These interacting dynamics create specific atmospheric circulation patterns that are together referred to as Combination Mode[65] (C-mode) (Box 1). The spatial pattern of the C-mode exhibits a pronounced hemispheric asymmetry, which includes an anomalous cyclonic low-level wind circulation in the Southern Hemisphere Central Pacific and an anomalous anticyclonic low-level wind circulation in the Northern Hemisphere Western Pacific. Some of prominent local expressions are the aforementioned southward shift of equatorial wind anomalies[64] (Figure 1e) and the anomalous Western North Pacific Anticyclone[66].

341

5) ENSO predictability

343 To link our dynamical understanding of tropical air-sea interactions with ENSO
344 predictability, it is helpful to elucidate the seasonal evolution of i) potential precursors
345 that may contribute to long-term predictability[67] (15-9 months lead time), ii) triggers
346 that can rapidly increase the likelihood for event development (9-6 months lead time)
347 and iii) transition processes (section 2, 4). The development of a typical EP event can be
348 divided into different seasonal stages which each contribute differently to the boreal
349 winter Niño 3.4 SSTA forecasting skill of up to 9-6 months, as illustrated by the anomaly
350 correlation coefficient skill between seasonal forecasts performed with the North
351 American Multimodel Ensemble[68] (NMME) and the observations (Figure 4a, cyan
352 dashed line). Prior to boreal spring a charged western tropical Pacific heat content is a
353 necessary condition for the subsequent development of El Niño events (Figure 4 b).
354 Corresponding warm pool heat advection processes[69,70] thus play a key role in
355 determining the long-term memory for ENSO forecasts. Furthermore, atmospheric
356 precursors in the North[39] and South Pacific[40], the Indian Ocean[71], or the tropical
357 Atlantic[42,72] have been suggested to influence the El Niño evolution for long lead times.

358

359 It must be emphasized here that the presence of such early oceanic or atmospheric
360 precursors is not sufficient for El Niño growth, as one of the key trigger mechanisms is
361 the stochastic WWE activity in boreal spring. Individual WWEs are not predictable
362 beyond the weather prediction horizon, which implies that on average forecasts
363 initialized in boreal spring have relatively low longterm skill[73] in particular in the
364 absence of pre-cursor signals (Figure 4a, cyan line). However, pre-cursor signals in
365 western tropical Pacific heat content (Figure 4b) could be indicative of potentially
366 developing El Niño conditions, which in effect raises the predictability (Figure 4a,
367 orange line), relative to the averaged case (Figure 4a, cyan line). The competing roles of
368 stochasticity versus ocean memory for this so-called spring predictability barrier
369 (Figure 4a) and for long-lead time forecasts have been intensely debated[74,75].

370

371 If a sufficient amount of westerly momentum is transferred in boreal spring from the
372 atmosphere to the ocean, zonal advective processes begin moving the warm pool front
373 eastward and downwelling Kelvin waves (Box 1) generate surface warming in the

374 eastern tropical Pacific about 2 months later. These anomalies will be further intensified
375 (Figure 4a) owing to increasing summer air-sea coupling strength (Figure 1j), while
376 anomalously warm water is drained from the Western Pacific Warm Pool (Figure 4b).
377 This phase exhibits a high degree of climate predictability, as documented by the high
378 anomaly correlation coefficients (>0.6) between predicted boreal winter El Niño events
379 and observations for forecasts initialized in boreal summer (Figure 4a). The subsequent
380 demise of an El Niño event is largely controlled by ocean-subsurface processes and the
381 discharge of zonal heat content away from the equator (Figure 1i, 2), as well as by the
382 seasonally modulated southward shift of westerly wind anomalies[64], which in turn leads
383 to a relaxation of the zonally integrated thermocline anomalies. This seasonally locked
384 decay of El Niño conditions under a low noise atmospheric environment further
385 contributes to the long-term averaged ENSO prediction skill[63].

386

387 The subsequent evolution into a La Niña state (Figure 4a,b) and the possibility to have
388 multi-year La Niña events (Figure 1k, 4c) are less well understood. La Niña events are
389 often preceded by a strong El Niño. However, as indicated by the broad probability
390 distribution of SSTA at lag 15-9 months (Figure 4c), other initial conditions can also
391 develop into La Niña events peaking in boreal winter (Figure 4c). During the transition
392 from El Niño to La Niña equatorial heat gets quickly discharged and 9-6 months prior to
393 a peak La Niña in boreal winter, we observe the smallest values of the equatorial heat
394 content (Figure 1i) and a slow recharging of the Western Pacific Warm Pool (Figure 4d).
395 However, also during this period the probability density of western tropical Pacific heat
396 content anomalies is relatively broad, which translates into an overall reduction of
397 predictive skill (Figure 4c). As longer-lasting La Niña events are exposed to a variety of
398 atmospheric and oceanic perturbations and the annual cycle, a dynamical decoupling of
399 La Niña and subsequent El Niño events may occur[76]. In boreal winter, during the peak of
400 the La Niña, Western Pacific Warm Pool is fully charged (Figure 4d) to values that are
401 typical for an El Niño pre-cursor (Figure 4b). However, the SST conditions do not
402 necessarily have to swing back to an El Niño state and sometimes even a second
403 subsequent La Niña can develop. Comparing the anomaly correlation coefficient skill for
404 December La Niña target conditions with the averaged skill for all years (1980-2015)
405 from the NMME[68], we find very little difference (Figure 4c) for lead times 12-1 month,
406 which suggests i) that La Niña conditions have a considerably lower predictability than

El Niño, ii) the predictability of La Niña is to a first order captured well by the mean statistical skill of the current generation of seasonal prediction models. Using ensemble forecasting techniques, a recent study[77] identified potential predictors for the likelihood of multi-year La Niña events, which include the magnitude of thermocline discharge and the amplitude of the preceding El Niño event, suggesting the possibility for longer-term forecasts also for La Niña.

How the different stages of predictability differ between CP and EP events and whether there are distinct precursor patterns for different ENSO flavors still remains controversial[69,78]. Despite an improved understanding of ENSO dynamics, ENSO prediction skill has not demonstrated a steady improvement during the past few decades, with even a decrease of ENSO prediction skill at the turn of the 21st Century[73]. This decrease may be related to the reduced ENSO amplitude and the more frequent occurrence of CP events during that period[78], as their evolution and climate impacts tend to be less predictable than those of EP El Niño events[79].

6) A unifying framework

The discussions in previous sections have highlighted a variety of dynamical pathways that can be synthesized to explain the spatio-temporal complexity of the ENSO phenomenon (Figure 5). Extending beyond the simple single mode theory (section 2), which captures several features of ENSO dynamics, but not all, our proposed framework for ENSO complexity is based on the co-existence of a duplet of linear eigenmodes (Figure 5 a,b), which can be derived from a coupled intermediate ENSO model[48], and a number of excitation mechanisms. These two modes are characterized by spatial patterns that closely resemble the observed EP and CP modes (Figure 5) and by timescales of approximately 4 and 2 years, respectively. The 4-year (quasi-quadrennial, QQ) mode is more prominent (Figure 5, lower left) when the mean thermocline is deep and the tradewinds are weak. It relies strongly on the thermocline feedback. In contrast, the 2-year mode (quasi-biennial, QB) is dominant when the mean thermocline is shallow and the equatorial trade winds are strong. Its SST variability is strongly controlled by the zonal advective feedback[48]. These features are akin to their observational counterparts (Figure 3, 5 c,d). For realistic background states both modes operate not far away from criticality (zero growth rate) (Figure 5, lower left), which

440   implies that they can be easily excited by other processes. Their stability and excitability

441   depends further on the prevailing climatic background conditions.

442

443   At the heart of our explanation for ENSO's *spatial* flavors is the aforementioned

444   multiplicity of coupled ENSO eigenmodes (Figure 5 a,b), as seen in intermediate ENSO

445   models[48]. Furthermore, the *temporal* complexity is generated in part by the different

446   oscillation frequencies of the QQ and QB modes and additionally by different external

447   excitation processes associated e.g. with the North and South Pacific Meridional

448   Modes[80,81], the South Pacific booster[40], Westerly Wind Events (section 3,4), Tropical

449   Instability Waves[82], or transbasin influences[42,83] (Figure 5). In particular, asymmetric

450   dependencies related to the increased Westerly Wind event activity during El Niño and

451   enhanced Tropical Instability Wave activity during La Niña make these cross scale

452   interactions very effective sources for ENSO complexity. Furthermore, the annual cycle

453   of winds and SST plays a key role in determining the seasonal timing of ENSO anomalies

454   and its predictability (section 4). To further explain the fact that El Niño anomalies are

455   stronger in amplitude (section 2) and exhibit a more pronounced spatial diversity

456   (section 3), and higher predictability[84] relative to their La Niña counterparts (Figure

457   4,b,d, 5c,e), we need to invoke additional nonlinear processes. Nonlinearities,

458   particularly in atmospheric deep convection and oceanic heat advection, can induce a

459   wide range of additional timescales[25] and new spatial structures[85,86] by potentially

460   coupling and/or amplifying the primary ENSO modes.

461

462   Decadal subsurface processes[87,88] can affect the long-term climatological background

463   state. In turn this will change the stability of the two primary ENSO eigenmodes (Figure

464   5 a,b) and their excitability. Hence, slow background state changes in the Pacific Ocean

465   can play a key role in generating and modulating ENSO's spatio-temporal complexity.

466

467   Our synthesis framework for ENSO complexity (Figure 5), which identifies key

468   ingredients for ENSO complexity (primary ENSO eigenmodes, excitation processes,

469   nonlinearities and cross-timescale interactions), may serve as a roadmap for further

470   hypotheses testing, process studies and diagnostic analysis of climate models. It can

471   help guide the evolution of the tropical Pacific observing system, which is an essential

472   underpinning of ENSO research and forecasting[89]. In addition, this framework can be

473 used to determine how the shortcomings in representing ENSO complexity in climate
474 and earth system models are related to a variety of feedback processes and biases in the
475 mean state and annual cycle that affect the generation of climate variability.
476

477 **7) Outlook**
478 The reliability of dynamical seasonal climate predictions depends heavily on the
479 representation of ENSO processes in CGCMs. Climate models still exhibit stubborn
480 climate biases in the eastern equatorial Pacific[90] that may impact their representation of
481 feedbacks (section 2), ENSO complexity[49], and in turn may affect the fidelity of
482 operational ENSO forecasts. Identifying and resolving underlying systematic model
483 biases will help in developing the next generation of models for seamless climate
484 forecasts and projections. Future research on ENSO complexity needs to address the
485 role of the seasonal cycle for CP ENSO dynamics, the near-absence of spatial diversity
486 for La Niña[31] (Figure 5e), the impact of decadal background state changes on ENSO
487 modes vis-à-vis multi-timescale processes involving Westerly Wind Events, Tropical
488 Instability waves and extratropical triggers and the response of ENSO's spatio-temporal
489 complexity to past and future climate change. Moreover, it needs to be studied, whether
490 the underlying dynamical origin for spatial-temporal diversity in CGCMs can in fact be
491 linked to the duplet of QQ and QB ENSO eigenmodes, described in section 6. This can be
492 tested by applying interactive atmosphere ensemble averaging techniques in coupled
493 climate models[91], which artificially reduce non-SST-related atmospheric perturbations.
494 Moreover, the use of flux-adjusted CGCMs[92] could help elucidate how model biases
495 impact ENSO's spatial diversity and provide a more effective way of improving seasonal
496 climate predictions. Such experiments could further reveal if there are distinct
497 precursors for ENSO diversity, which could be used to further inform ENSO forecasts.
498 Much scientific emphasis has been placed on understanding the growth of El Niño
499 events. However, given the severe impacts of La Niña e.g. on drought in the
500 Southwestern United States[93] or the Horn of Africa[94], and the fact that La Niña events
501 may last longer than one year (Figure 4), it will be paramount to gain also deeper
502 understanding of the processes controlling La Niña and its predictability through
503 observational, diagnostic and modeling studies.
504

505 A growing global population in the 21st century has become increasingly vulnerable to

natural hazards as human activities alter the climate and the environment. Society therefore has an urgent demand for better climate products and services, including improved seasonal ENSO predictions and long term projections, to better inform decision-making for agriculture and food security, public health, water resource management, energy production, human migration, and disaster risk reduction. ENSO is a unifying concept in earth system science[95]. Thus, our proposed synthesis for ENSO complexity (sections 2-5) can serve as both a catalyst to further research and, in its practical applications, an essential contributor for sustainable development and environmental stewardship in a changing world.

Figure 1| ENSO Cycle: Composite evolution of El Niño events from 1958 to 2015. a) Mean sea surface temperature[28] (SST) and b) subsurface potential temperature[96] between 2ºN and 2ºS. The depth of the 20ºC isotherm (Z20) is indicated by the black line. (c-h) Composite SST anomalies[28] (SSTA) and subsurface temperature anomalies[96] from 17 El Niño events (1963, 1965, 1968, 1969, 1972, 1976, 1977, 1982, 1986, 1987, 1991, 1994, 1997, 2002, 2004, 2006, 2009), based on the 0.5ºC exceedance of the three month running mean of NOAA ERSST.v2 SST anomalies[97] in the Niño3.4 region (averaged over 5ºS-5ºN, 120ºW-170ºW). The arrows schematically represent wind anomalies and the boxes list major processes involved in the phases of El Niño evolution. (i) The composite means (lines) and spread (shading) of Niño3 SSTA (red, averaged over 5ºS-5ºN, 90ºW-150ºW,) and equatorial Pacific zonal mean Z20 (blue) for the 17 El Niño events. The diamond illustrates that ENSO predictability increases with increasing ENSO signal strength. (j) The monthly standard deviation (SD) of Niño3 SSTA[28] (red line) and an estimate of monthly ENSO growth rate based on the Bjerknes stability index[57]. (k) Time series of Niño3 SSTA and zonal mean equatorial Pacific depth anomaly from 20ºC isotherm (from 2ºS-2ºN, 120ºE-80ºW) from merged data product[29,98].

Figure 2: | Schematic representation of ENSO temporal complexity. Orange shading show the kernel density estimate of the joint probability distribution of linearly detrended Niño3 SSTA and zonal mean 20ºC isotherm depth anomalies (from 2ºS-2ºN, 120ºE-80ºW) for the period 1958-2016 from a merged data product[29,98]. The gray circles

539   indicate the monthly values of the two time series, smoothed with a 3-month running
540   mean filter. Dark and light blue triangles indicate December values of EP (1972, 1982,
541   1986, 1997, 2006, 2015) and CP El Niños (1968, 1994, 2002, 2009). The years for the
542   four largest El Niño events are indicated. The white ellipse in the center corresponds to
543   the progression of the linear recharge oscillator, and arrows on the left and right
544   indicate (dis)charging of subsurface warm water in the equatorial Pacific.

545

546   **Figure 3. Spatio-temporal complexity of ENSO.** 1st (a) 2nd (b) EOF patterns of linearly
547   detrended SSTA[95] computed for 25°S-25°N, 140°E-80°W during 1920-2016, with
548   associated variance-preserving spectral power density on the left (vertical axis is period
549   in years, horizontal axis is log power); c,d,e) longitude-time evolution of Pacific SSTA
550   averaged 5°S-5°N, for selected observed ENSO events, with 28.5°C isotherm of SST (red
551   curve) representing the edge of the Western Pacific Warm Pool, longitude and strength
552   of WWEs[99] (black circles), and (on the left) associated equatorial Pacific heat content
553   anomaly (temperature anomaly averaged over the top 300 m of the ocean and between
554   5°S-5°N and 120°E-90°W; range from -1 to 1K; red positive, blue negative). The El Niño
555   of 1997/98 exhibits initially strong heat content, a strong eastward expansion of the
556   warm pool and WWE activity at El Niño onset in boreal spring and summer, and a
557   strong reduction of heat content after the event. In contrast, the El Niño of 2004/05
558   shows weaker initial heat content, less eastward expansion of WWE activity, and almost
559   no discharge of heat content[98] after the event. (f-m) spatial pattern of SSTA (shaded)
560   and precipitation anomaly[100] (contours, positive solid, negative dashed, 2 mm/day
561   interval, zero contour omitted) averaged over the Nov-Dec-Jan season of selected ENSO
562   events.   Note that strong warm events (1997/98, 2015/16) induce very strong
563   eastward and equatorward shifts of rainfall. Bottom-right of each panel of (a,b,f-m)
564   shows the associated principal components (PCs), namely the projection of each SSTA
565   spatial pattern onto the EOF patterns in (a,b); abscissa is PC1, ordinate is PC2, and
566   arrow length is relative to the unit circle.

567   .

568   **Figure 4 | Probabilistic ENSO pre-cursors and predictive skill.** Kernel-density probability
569   density estimates of linearly detrended Niño3.4 SSTA[28] for the period 1958-2016 for a.)
570   El Niño and b.) La Niña conditions, exceeding the +/-0.5°C threshold
571   (White/transparent shading), respectively. c.) and d.) same as a.), b.), but for western

572 tropical Pacific heat content anomalies[96] (temperature anomalies averaged from 5ºS-
573 5ºN, 120ºE-155ºW and 0-300 m and high-pass filtered with a cut-off period of 20 years
574 to remove multi-decadal trends). The time-evolution of the probability density
575 estimates is shown for different lead and lag times, relative to El Niño and La Niña
576 events peaking in December. Colored think lines correspond to the maximum
577 probability for each lag. Thick lines in a.) represent the anomaly correlation coefficient
578 skill (ACC) for December Niño3.4 SSTA[97] (1980-2015) exceeding +0.5ºC (orange),
579 within the range +/-0.5ºC (gray) and for all years (cyan) as calculated using 9 coupled
580 models from the North American Multimodel Ensemble project[68]. Lines in b.), same as
581 a.), but for anomalies below -0.5ºC (blue), within the range +/-0.5ºC (gray) and all
582 years (cyan).

583

584 Figure 5 | Mechanisms for ENSO Complexity. Top two left panels: Leading modes of SSTA
585 (ºC) and equatorial thermocline depth anomalies (averaged between 5ºS-5ºN, unit in
586 meters) with periods of ~4 (QQ) and ~2 (QB) year, as obtained from the eigenanalysis
587 of an intermediate ENSO model[48]. The differences in zonal location of the center in SSTA
588 and thermocline anomalies are largely due to the different magnitude and spatial
589 characteristics of the zonal advective feedback (ZAF) and thermocline feedback (TF).
590 Bottom two panels on the left: growth rates (unit: 1/year) of the co-existing two leading
591 ENSO modes as a functions of mean thermocline depth and the strength of mean
592 equatorial trade winds relative to climatological conditions. The black dots mark the
593 mean state condition for the modes displayed in the two panels above. Right panels:
594 patterns of SSTA[28] and top 300m heat content anomalies (unit: 10^{10} J/m^2) averaged
595 between 5ºS-5ºN for typical EP (1997/98), CP (2009/2010) El Niño, and La Niña
596 (boreal winter 2010) events (Nov-Dec-Jan) with schematic representation of key
597 excitation, nonlinear and cross-scale interaction mechanisms: annual cycle (ACY),
598 Westerly Wind Events (WWE), South Pacific Booster (SPB), North and South Pacific
599 Meridional Modes (NPMM, SPMM) and Tropical Instabilty Waves (TIW). Note the
600 similarity between observed (right) and theoretical (left) SSTA patterns and relative
601 amplitude of feedbacks. The observations also exhibit a striking asymmetry between El
602 Niño and La Niña spatial diversity, owing to the presence of nonlinear processes. ENSO
603 complexity is also affected by decadal-scale changes of the equatorial background state,
604 atmospheric influences originating from Indian Ocean and Atlantic Ocean SSTA, and

605 other external forcings. The solid red-eastward (blue-westward) arrows represent the
606 ZAF and red-upward (blue-downward) TF for El Niño (La Niña) conditions,
607 respectively. The relative sizes and different zonal positions of the arrows indicate
608 qualitatively the strength and areas of strong feedback efficiency. Curly upward
609 (downward) arrows denote the damping net surface heat flux feedback for El Niño (La
610 Niña). Thermocline processes are characterized by heat content anomalies averaged
611 over the upper 300 m in the right panels and depth anomalies of the 20°C isotherm in
612 the left panels.
613
614
615 **Box 1| ENSO Glossary:**
616
617 **Bjerknes feedback:** Positive (reinforcing) ENSO feedback along the equator, in which a
618 weakened equatorial zonal SST gradient weakens trade winds, which in turn further
619 reduces the zonal SST gradient due to the balance of ocean dynamical and
620 thermodynamical processes. The Bjerknes feedback is seasonally modulated and peaks
621 in late boreal summer to fall. The Bjerknes feedback also tends to intensify the growth
622 of La Niña events.
623 **Combination Tones / C-mode:** Enhanced spectral energy on timescales of 9 months and
624 15-18 months, generated by the nonlinear modulation of ENSO by the seasonal cycle,
625 and vice versa. This interaction plays an important part in the seasonal turnabout of El
626 Niño events and in establishing the linkage between ENSO and the East Asian Monsoon
627 system.
628 **Eastern Pacific Cold Tongue:** An eastern equatorial Pacific region characterized by wind-
629 driven upwelling of cold subsurface waters (Figure 1a,b). The Cold Tongue warms
630 considerably during Eastern Pacific (EP) El Niño events, and cools during La Niña
631 events. The subsiding branch of the atmospheric Walker Circulation is located over the
632 Cold Tongue.
633 **Ekman Feedback:** Positive (negative) SST anomalies weaken (strengthen) the equatorial
634 trade winds, reducing (increasing) the upwelling of cold subsurface water in the eastern
635 equatorial Pacific, thus reinforcing the original SST anomaly.
636 **ENSO Complexity**: Complexity expands on the concept of ENSO "pattern diversity" to
637 include also temporal characteristics, dynamics, predictability and global impacts. ENSO

638   complexity arises from processes operating on a variety of timescales (from weather,
639   annual cycle, interannual to decadal timescales).

640   **ENSO Skewness:** Amplitude asymmetry of El Niño and La Niña events, which quantifies
641   the fact that El Niño events attain larger amplitudes than La Niña events. Skewness is
642   clear indication of nonlinearity in the ENSO cycle.

643   **Equatorial Kelvin Wave:** Eastward propagating oceanic internal wave that displaces the
644   interface (thermocline) between warm surface waters and cold subsurface waters.
645   Westerly equatorial wind anomalies generate downwelling Kelvin waves, which deepen
646   the thermocline in the eastern Pacific and thus reduce the efficiency of cooling by
647   climatological upwelling in the eastern Pacific. The opposite occurs for easterly wind
648   anomalies. Kelvin waves need about 2 months to propagate across the equatorial
649   Pacific.

650   **Multiplicative Noise:** Interaction between Westerly Wind Events (WWEs) and
651   underlying SST in the western and central Pacific, in which warmer (colder) SST favors
652   more (fewer) WWEs, also referred to as state-dependent noise.

653   **Recharge/Discharge**: Meridional transport of heat into/out of equatorial band driven by
654   changes in near-equatorial wind variations. Recharge/discharge processes plays key
655   role in initiation and termination of El Niño events.

656   **Thermal damping**: Typically a negative feedback arising from SST-induced changes in
657   surface radiative and turbulent heat fluxes in the tropical Pacific. It involves tropical
658   clouds, convection and atmospheric boundary layer physics.

659   **Thermocline feedback**: Generally positive feedback operating in the eastern equatorial
660   Pacific, in which a warm (cold) equatorial SSTA weakens (strengthens) equatorial trade
661   winds, leading to mean upwelling of anomalously warm (cold) water.

662   **Westerly Wind Event:** Weather systems in the western and central Pacific, that are often
663   associated with an abrupt relaxation of the equatorial trade winds, generating
664   downwelling Kelvin waves and an eastward expansion of the Western Pacific Warm
665   Pool. WWEs play a central role in triggering and amplifying El Niño events.

666   **Western Pacific Warm Pool:** Some of the warmest waters in the worlds' oceans occur in
667   the western tropical Pacific with temperatures exceeding 28°C (Figure 1a,b). The Warm
668   Pool's seasonal north-south migrations and their influence on the atmosphere play an
669   important role in equatorial air-sea coupling, and in the termination of El Niño events.

670   **Zonal-advective feedback**: Positive feedback, particularly effective in the central Pacific,

in which a positive (negative) equatorial SSTA weakens (strengthens) equatorial trade winds, reducing (enhancing) the oceanic transport of cold waters from the eastern Pacific.

1   Carrillo, C. N. Hidrografía oceánica. *Bol Soc Geogr Lima*, 72-110 (1893).

2   Bjerknes, J. Atmospheric Teleconnections from the Equatorial Pacific. *Monthly Weather Review* **97**, 163-172 (1969).

3   McPhaden, M. J., Busalacchi, A. J. & Anderson, D. L. T. A TOGA Retrospective. *Oceanography* **23**, 86-103, doi:10.5670/oceanog.2010.26 (2010).

4   Cai, W. J. *et al.* More extreme swings of the South Pacific convergence zone due to greenhouse warming. *Nature* **488**, 365-369, doi:10.1038/nature11358 (2012).

5   Capotondi, A. *et al.* Understanding ENSO Diversity. *Bulletin of the American Meteorological Society* **96**, 921-938, doi:10.1175/bams-d-13-00117.1 (2015).

703 6 Kug, J. S., Jin, F. F. & An, S. I. Two Types of El Niño Events: Cold Tongue El Niño
704   and Warm Pool El Niño. *Journal of Climate* **22**, 1499-1515,
705   doi:10.1175/2008jcli2624.1 (2009).
706 **Demonstrates that the two types of El Niño (CP and EP) have different dynamical**
707   **structures including discharge processes and dominant SST feedbacks.**
708 7 Ashok, K., Behera, S. K., Rao, S. A., Weng, H. Y. & Yamagata, T. El Niño Modoki and
709   its possible teleconnection. *Journal of Geophysical Research-Oceans* **112**,
710   doi:10.1029/2006jc003798 (2007).
711 8 Takahashi, K., Montecinos, A., Goubanova, K. & Dewitte, B. ENSO regimes:
712   Reinterpreting the canonical and Modoki El Niño. *Geophysical Research Letters*
713   **38**, doi:10.1029/2011gl047364 (2011).
714 9 Tziperman, E. & Yu, L. S. Quantifying the dependence of westerly wind bursts on
715   the large-scale tropical Pacific SST. *Journal of Climate* **20**, 2760-2768,
716   doi:10.1175/jcli4138.1 (2007).
717 10 Lengaigne, M. *et al.* Triggering of El Niño by westerly wind events in a coupled
718   general circulation model. *Climate Dynamics* **23**, 601-620, doi:10.1007/s00382-
719   004-0457-2 (2004).
720 11 Timmermann, A. Decadal ENSO amplitude modulations: a nonlinear paradigm.
721   *Global and Planetary Change* **37**, 135-156, doi:10.1016/S0921-8181(02)00194-7
722   (2003).
723 12 Choi, J., An, S. I. & Yeh, S. W. Decadal amplitude modulation of two types of ENSO
724   and its relationship with the mean state. *Climate Dynamics* **38**, 2631-2644,
725   doi:10.1007/s00382-011-1186-y (2012).
726 13 L'Heureux, M. L. *et al.* Observing and predicting the 2015/16 El Niño. *Bulletin of*
727   *the American Meteorological Society* **98**, 1363-1382, doi:10.1175/bams-d-16-
728   0009.1 (2017).
729 14 Jin, F. F., Kim, S. T. & Bejarano, L. A coupled-stability index for ENSO. *Geophysical*
730   *Research Letters* **33**, doi:10.1029/2006gl027221 (2006).
731 15 Hoerling, M. P. & Kumar, A. Why do North American climate anomalies differ
732   from one El Niño event to another? *Geophysical Research Letters* **24**, 1059-1062,
733   doi:10.1029/97gl00918 (1997).
734 16 Karoly, D. J. & Hoskins, B. J. 3 dimensional Propagation of Planetary Waves.
735   *Journal of the Meteorological Society of Japan* **60**, 109-123 (1982).

736   17   Ropelewski, C. F. & Halpert, M. S. Global and Regional Scale Precipitation
737   Patterns associated with the El-Niño Southern Oscillation. *Monthly Weather*
738   *Review* **115**, 1606-1626, (1987).
739   18   Larkin, N. K. & Harrison, D. E. On the definition of El Niño and associated
740   seasonal average US weather anomalies. *Geophysical Research Letters* **32**, 4,
741   doi:10.1029/2005gl022738 (2005).
742   19   Cobb, K. M. *et al.* Highly Variable El Niño-Southern Oscillation Throughout the
743   Holocene. *Science* **339**, 67-70, doi:10.1126/science.1228246 (2013).
744   20   McGregor, S., Timmermann, A., England, M. H., Timm, O. E. & Wittenberg, A. T.
745   Inferred changes in El Niño-Southern Oscillation variance over the past six
746   centuries. *Climate of the Past* **9**, 2269-2284, doi:10.5194/cp-9-2269-2013
747   (2013).
748   **Documents using multi-proxy data that ENSO variance has increased over the past**
749   **Century, relative to the 500 years prior to this.**
750   21   Cai, W. J. *et al.* ENSO and greenhouse warming. *Nature Climate Change* **5**, 849-
751   859, doi:10.1038/nclimate2743 (2015).
752   22   Rasmusson, E. M. & Carpenter, T. H. Variations in Tropical Sea-Surface
753   Temperature and Surface Wind Fields associated with the Southern Oscillation
754   El-Niño. *Monthly Weather Review* **110**, 354-384, (1982).
755   23   Battisti, D. S. & Hirst, A. C. Interannual Variability in a Tropical Atmosphere
756   Ocean Model - Influence of the Basic State, Ocean Geometry and Nonlinearity.
757   *Journal of the Atmospheric Sciences* **46**, 1687-1712, (1989).
758   24   Jin, F. F. An equatorial ocean recharge paradigm for ENSO. Part I: Conceptual
759   model. *Journal of the Atmospheric Sciences* **54**, 811-829, (1997).
760   **Introduces heuristic model that explains key features of ENSO dynamics, such as the**
761   **important role of recharge and discharge processes in ENSO.**
762   25   Roberts, A., Guckenheimer, J., Widiasih, E., Timmermann, A. & Jones, C. Mixed-
763   Mode Oscillations of El Niño-Southern Oscillation. *Journal of the Atmospheric*
764   *Sciences* **73**, 1755-1766, doi:10.1175/jas-d-15-0191.1 (2016).
765   26   Levine, A. F. Z. & Jin, F. F. Noise-Induced Instability in the ENSO Recharge
766   Oscillator. *Journal of the Atmospheric Sciences* **67**, 529-542,
767   doi:10.1175/2009jas3213.1 (2010).

768   27   Kao, H. Y. & Yu, J. Y. Contrasting Eastern-Pacific and Central-Pacific Types of
769   ENSO. *Journal of Climate* **22**, 615-632, doi:10.1175/2008jcli2309.1 (2009).

770   28   Rayner, N. A. *et al.* Global analyses of sea surface temperature, sea ice, and night
771   marine air temperature since the late nineteenth century. *Journal of Geophysical*
772   *Research-Atmospheres* **108**, 4407, doi:10.1029/2002jd002670 (2003).

773   29   Giese, B. S. & Ray, S. El Niño variability in simple ocean data assimilation (SODA),
774   1871-2008. *Journal of Geophysical Research-Oceans* **116**,
775   doi:10.1029/2010jc006695 (2011).

776   30   Johnson, N. C. How Many ENSO Flavors Can We Distinguish? *Journal of Climate*
777   **26**, 4816-4827, doi:10.1175/jcli-d-12-00649.1 (2013).

778   31   Kug, J. S. & Ham, Y. G. Are there two types of La Niña? *Geophysical Research*
779   *Letters* **38**, doi:10.1029/2011gl048237 (2011).

780   32   Lengaigne, M. & Vecchi, G. A. Contrasting the termination of moderate and
781   extreme El Niño events in coupled general circulation models. *Climate Dynamics*
782   **35**, 299-313, doi:10.1007/s00382-009-0562-3 (2010).

783   33   An, S.-I., Kug, J.-S., Timmermann, A., Kang, I.-S. & Timm, O. The influence of ENSO
784   on the generation of decadal variability in the North Pacific. *Journal of Climate*
785   **20**, 667-680, doi:10.1175/JCLI4017.1 (2007).

786   34   Deser, C., Simpson, I. R., McKinnon, K. A. & Phillips, A. S. The Northern
787   Hemisphere Extratropical Atmospheric Circulation Response to ENSO: How Well
788   Do We Know It and How Do We Evaluate Models Accordingly? *Journal of Climate*
789   **30**, 5059-5082, doi:10.1175/jcli-d-16-0844.1 (2017).

790   35   Fedorov, A. V., Hu, S. N., Lengaigne, M. & Guilyardi, E. The impact of westerly
791   wind bursts and ocean initial state on the development, and diversity of El Niño
792   events. *Climate Dynamics* **44**, 1381-1401, doi:10.1007/s00382-014-2126-4
793   (2015).

794   36   Chen, D. K. *et al.* Strong influence of westerly wind bursts on El Niño diversity.
795   *Nature Geoscience* **8**, 339-345, doi:10.1038/ngeo2399 (2015).

796   37   Seiki, A. & Takayabu, Y. N. Westerly wind bursts and their relationship with
797   intraseasonal variations and ENSO. Part I: Statistics. *Monthly Weather Review*
798   **135**, 3325-3345, doi:10.1175/mwr3477.1 (2007).

799   38   Jin, F. F., Lin, L., Timmermann, A. & Zhao, J. Ensemble-mean dynamics of the
800   ENSO recharge oscillator under state-dependent stochastic forcing. *Geophysical*
801   *Research Letters* **34**, L03807, doi:10.1029/2006gl027372 (2007).
802   39   Vimont, D. J., Battisti, D. S. & Hirst, A. C. The seasonal footprinting mechanism in
803   the CSIRO general circulation models. *Journal of Climate* **16**, 2653-2667, (2003).
804   **Presents a coupled air-sea mechanisms by which extratropical Pacific climate anomalies**
805   **can propagate into the tropics**
806   40   Hong, L. C., LinHo & Jin, F. F. A Southern Hemisphere booster of super El Niño.
807   *Geophysical Research Letters* **41**, 2142-2149, doi:10.1002/2014gl059370
808   (2014).
809   41   Ham, Y. G., Kug, J. S., Park, J. Y. & Jin, F. F. Sea surface temperature in the north
810   tropical Atlantic as a trigger for El Niño/Southern Oscillation events. *Nature*
811   *Geoscience* **6**, 112-116, doi:10.1038/ngeo1686 (2013).
812   42   Chikamoto, Y. *et al.* Skilful multi-year predictions of tropical trans-basin climate
813   variability. *Nature Communications* **6**, doi:10.1038/ncomms7869 (2015).
814   **Documents the impact of Atlantic SST anomalies on the generation of CP El Niño events**
815   43   Yu, J. Y. & Kim, S. T. Relationships between Extratropical Sea Level Pressure
816   Variations and the Central Pacific and Eastern Pacific Types of ENSO. *Journal of*
817   *Climate* **24**, 708-720, doi:10.1175/2010jcli3688.1 (2011).
818   44   Lee, T. & McPhaden, M. J. Increasing intensity of El Niño in the central-equatorial
819   Pacific. *Geophysical Research Letters* **37**, doi:10.1029/2010gl044007 (2010).
820   45   Wittenberg, A. T., Rosati, A., Delworth, T. L., Vecchi, G. A. & Zeng, F. R. ENSO
821   Modulation: Is It Decadally Predictable? *Journal of Climate* **27**, 2667-2681,
822   doi:10.1175/jcli-d-13-00577.1 (2014).
823   46   Yeh, S. W. *et al.* El Niño in a changing climate. *Nature* **461**, 511-514,
824   doi:10.1038/nature08316 (2009).
825   47   Capotondi, A. & Sardeshmukh, P. D. Optimal precursors of different types of
826   ENSO events. *Geophysical Research Letters* **42**, 9952-9960,
827   doi:10.1002/2015gl066171 (2015).
828   48   Xie, R. & Jin, F.-F. Two Leading ENSO Modes and El Niño Types in the Zebiak-
829   Cane Model *Journal of Climate*, doi:10.1175/JCLI-D-1117-0469.1 (2018).
830   **Theoretical evidence for two coupled modes which resemble EP and CP El Niño events**
831   **with different timescales and background state sensitivities**

832   49   Ham, Y. G. & Kug, J. S. How well do current climate models simulate two types of
833   El Niño? *Climate Dynamics* **39**, 383-398, doi:10.1007/s00382-011-1157-3
834   (2012).
835   **Shows that the current generation of climate models tends to underestimate diversity of**
836   **El Niño due dry and cold biases in the equatorial central Pacific**
837   50   Bellenger, H., Guilyardi, E., Leloup, J., Lengaigne, M. & Vialard, J. ENSO
838   representation in climate models: from CMIP3 to CMIP5. *Climate Dynamics* **42**,
839   1999-2018, doi:10.1007/s00382-013-1783-z (2014).
840   51   Bayr, T. *et al.* Mean-state dependence of ENSO atmospheric feedbacks in climate
841   models. *Climate Dynamics*, doi:10.1007/s00382-00017-03799-00382 (2017).
842   52   Li, T. Phase transition of the El Niño Southern oscillation: A stationary SST mode.
843   *Journal of the Atmospheric Sciences* **54**, 2872-2887 (1997).
844   **Applies seasonally varying instability to model of coupled ENSO dynamics.**
845   53   Zhang, W. J. *et al.* Unraveling El Niño's impact on the East Asian Monsoon and
846   Yangtze River summer flooding. *Geophysical Research Letters* **43**, 11375-11382,
847   doi:10.1002/2016gl071190 (2016).
848   54   Trenberth, K. E. *et al.* Progress during TOGA in understanding and modeling
849   global teleconnections associated with tropical sea surface temperatures. *Journal*
850   *of Geophysical Research-Oceans* **103**, 14291-14324, doi:10.1029/97jc01444
851   (1998).
852   55   Risbey, J. S., Pook, M. J., McIntosh, P. C., Wheeler, M. C. & Hendon, H. H. On the
853   Remote Drivers of Rainfall Variability in Australia. *Monthly Weather Review* **137**,
854   3233-3253, doi:10.1175/2009mwr2861.1 (2009).
855   56   Vecchi, G. A. & Harrison, D. E. Tropical Pacific sea surface temperature anomalies,
856   El Niño, and equatorial westerly wind events. *Journal of Climate* **13**, 1814-1830,
857   (2000).
858   57   Wengel, C., Latif, M., Park, W., Harlass, J. & Bayr, T. Seasonal ENSO phase locking
859   in the Kiel Climate Model: The importance of the equatorial cold sea surface
860   temperature bias. *Climate Dynamics*, doi:10.1007/s00382-00017-03648-00383
861   (2017).
862   58   Zebiak, S. E. & Cane, M. A. A Model El-Niño Southern Oscillation. *Monthly*
863   *Weather Review* **115**, 2262-2278, (1987).

864   59   Tziperman, E., Zebiak, S. E. & Cane, M. A. Mechanisms of seasonal - ENSO
865   interaction. *Journal of the Atmospheric Sciences* **54**, 61-71, (1997).

866   60   Galanti, E. *et al.* The equatorial thermocline outcropping - A seasonal control on
867   the tropical Pacific Ocean-atmosphere instability strength. *Journal of Climate* **15**,
868   2721-2739, (2002).

869   61   Dommenget, D. & Yu, Y. S. The seasonally changing cloud feedbacks contribution
870   to the ENSO seasonal phase-locking. *Climate Dynamics* **47**, 3661-3672,
871   doi:10.1007/s00382-016-3034-6 (2016).

872   62   Harrison, D. E. & Vecchi, G. A. On the termination of El Niño. *Geophysical*
873   *Research Letters* **26**, 1593-1596, doi:10.1029/1999gl900316 (1999).

874   63   Lengaigne, M., Boulanger, J. P., Menkes, C. & Spencer, H. Influence of the seasonal
875   cycle on the termination of El Niño events in a coupled general circulation model.
876   *Journal of Climate* **19**, 1850-1868, doi:10.1175/jcli3706.1 (2006).

877   64   McGregor, S., Timmermann, A., Schneider, N., Stuecker, M. F. & England, M. H. The
878   Effect of the South Pacific Convergence Zone on the Termination of El Niño
879   Events and the Meridional Asymmetry of ENSO. *Journal of Climate* **25**, 5566-
880   5586, doi:10.1175/jcli-d-11-00332.1 (2012).

881   **Demonstrates that the southward wind-shift that leads to rapid decay of El Niño events is**
882   **related to the seasonal formation of the South Pacific Convergence Zone**

883   65   Stuecker, M. F., Timmermann, A., Jin, F. F., McGregor, S. & Ren, H. L. A
884   combination mode of the annual cycle and the El Niño/Southern Oscillation.
885   *Nature Geoscience* **6**, 540-544, doi:10.1038/ngeo1826 (2013).

886   66   Stuecker, M. F., Jin, F. F., Timmermann, A. & McGregor, S. Combination Mode
887   Dynamics of the Anomalous Northwest Pacific Anticyclone. *Journal of Climate* **28**,
888   1093-1111, doi:10.1175/jcli-d-14-00225.1 (2015).

889   67   Meinen, C. S. & McPhaden, M. J. Observations of warm water volume changes in
890   the equatorial Pacific and their relationship to El Niño and La Niña. *Journal of*
891   *Climate* **13**, 3551-3559, (2000).

892   68   Barnston, A. G. & Tippett, M. K. Do Statistical Pattern Corrections Improve
893   Seasonal Climate Predictions in the North American Multimodel Ensemble
894   Models? *Journal of Climate* **30**, 8335-8355, doi:10.1175/jcli-d-17-0054.1 (2017).

895   69   Ramesh, N. & Murtugudde, R. All flavours of El Niño have similar early
896   subsurface origins. *Nature Climate Change* **3**, 42-46 (2013).

897 70   Ballester, J., Bordoni, S., Petrova, D. & Rodo, X. Heat advection processes leading
898   to El Niño events as depicted by an ensemble of ocean assimilation products.
899   *Journal of Geophysical Research-Oceans* **121**, 3710-3729,
900   doi:10.1002/2016jc011718 (2016).
901 71   Izumo, T. *et al.* Influence of the state of the Indian Ocean Dipole on the following
902   year's El Niño. *Nature Geoscience* **3**, 168-172, doi:10.1038/ngeo760 (2010).
903 72   Ham, Y. G., Kug, J. S. & Park, J. Y. Two distinct roles of Atlantic SSTs in ENSO
904   variability: North Tropical Atlantic SST and Atlantic Niño. *Geophysical Research*
905   *Letters* **40**, 4012-4017, doi:10.1002/grl.50729 (2013).
906 73   Barnston, A. G., Tippett, M. K., L'Heureux, M. L., Li, S. H. & DeWitt, D. G. Skill of
907   Real-Time Seasonal ENSO Model Predictions during 2002-11: Is Our Capability
908   Increasing? *Bulletin of the American Meteorological Society* **93**, 631-651,
909   doi:10.1175/bams-d-11-00111.1 (2012).
910 74   Newman, M. & Sardeshmukh, P. D. Are we near the predictability limit of tropical
911   Indo-Pacific sea surface temperatures? *Geophysical Research Letters* **44**, 8520-
912   8529, doi:10.1002/2017gl074088 (2017).
913 75   Petrova, D., Koopman, S. J., Ballester, J. & Rodo, X. Improving the long-lead
914   predictability of El Niño using a novel forecasting scheme based on a dynamic
915   components model. *Climate Dynamics* **48**, 1249-1276, doi:10.1007/s00382-016-
916   3139-y (2017).
917 76   Kessler, W. S. Is ENSO a cycle or a series of events? *Geophysical Research Letters*
918   **29**, doi:10.1029/2002gl015924 (2002).
919   **Challenges the notion of ENSO as a cycle and highlights the fact that the ENSO system can**
920   **loose its dynamical memory during long La Niña events**
921 77   DiNezio, P. N., Deser, C., Okumura, Y. & Karspeck, A. Predictability of 2-year La
922   Niña events in a coupled general circulation model. *Climate Dynamics* **49**, 4237-
923   4261, doi:10.1007/s00382-017-3575-3 (2017).
924 78   McPhaden, M. J. A 21st century shift in the relationship between ENSO SST and
925   warm water volume anomalies. *Geophysical Research Letters* **39**,
926   doi:10.1029/2012gl051826 (2012).
927 79   Jeong, H. I. *et al.* Assessment of the APCC coupled MME suite in predicting the
928   distinctive climate impacts of two flavors of ENSO during boreal winter. *Climate*
929   *Dynamics* **39**, 475-493, doi:10.1007/s00382-012-1359-3 (2012).

930   80   Larson, S. & Kirtman, B. The Pacific Meridional Mode as a trigger for ENSO in a
931   high-resolution coupled model. *Geophysical Research Letters* **40**, 3189-3194,
932   doi:10.1002/grl.50571 (2013).

933   81   Zhang, H. H., Clement, A. & Di Nezio, P. The South Pacific Meridional Mode: A
934   Mechanism for ENSO-like Variability. *Journal of Climate* **27**, 769-783,
935   doi:10.1175/jcli-d-13-00082.1 (2014).

936   82   An, S. I. Interannual variations of the Tropical Ocean instability wave and ENSO.
937   *Journal of Climate* **21**, 3680-3686, doi:10.1175/2008jcli1701.1 (2008).

938   83   Okumura, Y. M. & Deser, C. Asymmetry in the Duration of El Niño and La Niña.
939   *Journal of Climate* **23**, 5826-5843, doi:10.1175/2010jcli3592.1 (2010).

940   84   Larson, S. M. & Kirtman, B. P. Linking preconditioning to extreme ENSO events
941   and reduced ensemble spread. *Climate Dynamics*, doi:10.1007/s00382-00017-
942   03791-x (2017).

943   85   Chen, N. & Majda, A. J. Simple dynamical models capturing the key features of the
944   Central Pacific El Niño. *Proceedings of the National Academy of Sciences of the*
945   *United States of America* **113**, 11732-11737, doi:10.1073/pnas.1614533113
946   (2016).

947   86   Hao, Z., Neelin, J. D. & Jin, F. F. Nonlinear Tropical Air-Ssea Interaction in the Fast-
948   Wave Limit. *Journal of Climate* **6**, 1523-1544, (1993).

949   87   Schneider, N. The response of tropical climate to the equatorial emergence of
950   spiciness anomalies. *Journal of Climate* **17**, 1083-1095, (2004).

951   88   McGregor, S., Sen Gupta, A., Holbrook, N. J. & Power, S. B. The Modulation of ENSO
952   Variability in CCSM3 by Extratropical Rossby Waves. *Journal of Climate* **22**, 5839-
953   5853, doi:10.1175/2009jcli2922.1 (2009).

954   89   Xue, Y. *et al.* A real-time ocean reanalyses intercomparison project in the context
955   of Tropical Pacific observing system and ENSO monitoring. *Climate Dynamics* **49**,
956   3647-3672, doi:10.1007/s00382-017-3535-y (2017).

957   90   Widlansky, M. J. *et al.* Changes in South Pacific rainfall bands in a warming
958   climate. *Nature Climate Change* **3**, 417-423, doi:10.1038/NCLIMATE1726
959   (2013).

960   91   Kirtman, B. P., Straus, D. M., Min, D. H., Schneider, E. K. & Siqueira, L. Toward
961   linking weather and climate in the interactive ensemble NCAR climate model.
962   *Geophysical Research Letters* **36**, doi:10.1029/2009gl038389 (2009).

963   92   Vecchi, G. A. *et al.* On the Seasonal Forecasting of Regional Tropical Cyclone
964   Activity. *Journal of Climate* **27**, 7994-8016, doi:10.1175/jcli-d-14-00158.1
965   (2014).
966   93   Cook, E. R., Seager, R., Cane, M. A. & Stahle, D. W. North American drought:
967   Reconstructions, causes, and consequences. *Earth-Science Reviews* **81**, 93-134,
968   doi:10.1016/j.earscirev.2006.12.002 (2007).
969   94   Nicholson, S. E. & Selato, J. C. The influence of La Niña on African rainfall.
970   *International Journal of Climatology* **20**, 1761-1776, (2000).
971   95   McPhaden, M. J., Zebiak, S. E. & Glantz, M. H. ENSO as an integrating concept in
972   Earth science. *Science* **314**, 1740-1745, doi:10.1126/science.1132588 (2006).
973   96   Balmaseda, M. A., Mogensen, K. & Weaver, A. T. Evaluation of the ECMWF ocean
974   reanalysis system ORAS4. *Quarterly Journal of the Royal Meteorological Society*
975   **139**, 1132-1161, doi:10.1002/qj.2063 (2013).
976   97   Huang, B. Y. *et al.* Extended Reconstructed Sea Surface Temperature, Version 5
977   (ERSSTv5): Upgrades, Validations, and Intercomparisons. *Journal of Climate* **30**,
978   8179-8205, doi:10.1175/jcli-d-16-0836.1 (2017).
979   98   Penny, S. G., Behringer, D. W., Carton, J. A. & Kalnay, E. A Hybrid Global Ocean
980   Data Assimilation System at NCEP. *Monthly Weather Review* **143**, 4660-4677,
981   doi:10.1175/mwr-d-14-00376.1 (2015).
982

a) Mean sea surface temperature
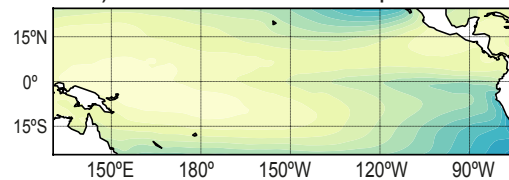
b) Mean subsurface temperature, 2ºS-2ºN

Temperature (ºC)
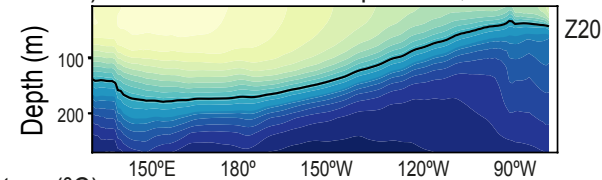
h) Mature La Niña   December Year 1

Bjerknes feedbacks | More cold water upwelling to surface

i)

Predictability

c) Onset   April Year 0

Stochasitc forcing (WWEs) | Downwelling Kelvin waves
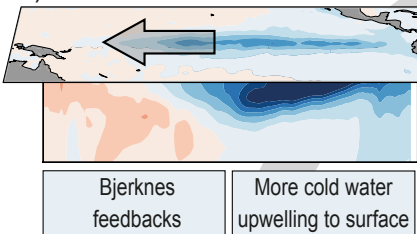
g) Transition   August Year 1

Upwelling Kelvin waves

j)

d) Growth   August Year 0

Nonlinear Bjerknes feedbacks
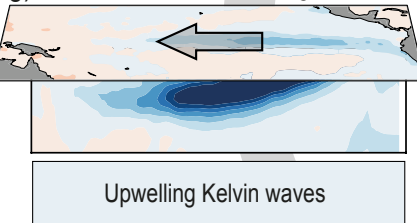
f) Decay   April Year 1

Discharging of heat content
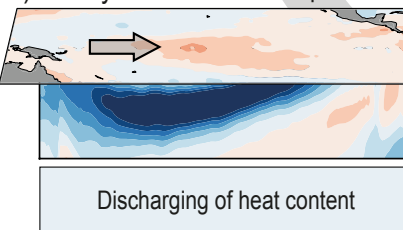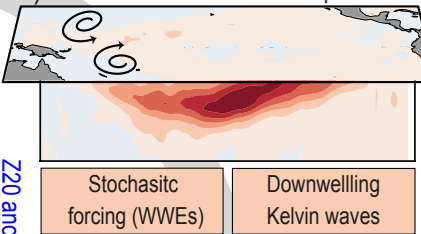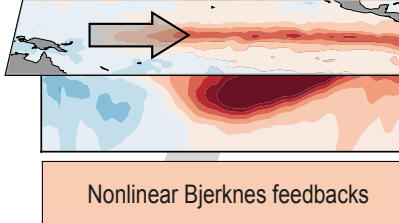
e) Mature El Niño   December Year 0

Southward shift of wind anomalies

Temperature anomaly (ºC)

k)
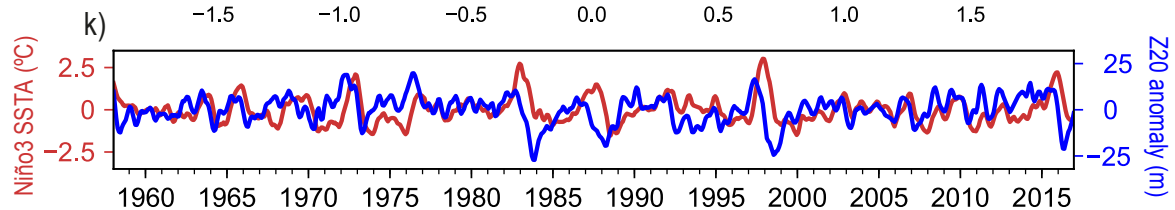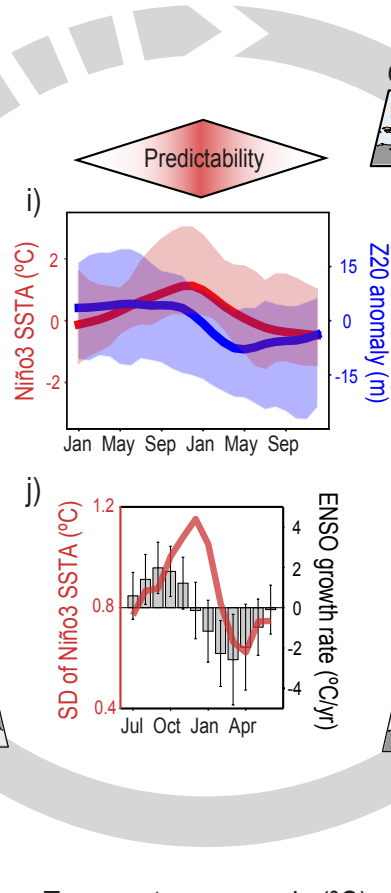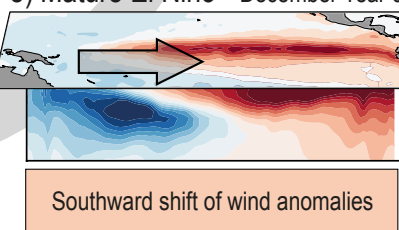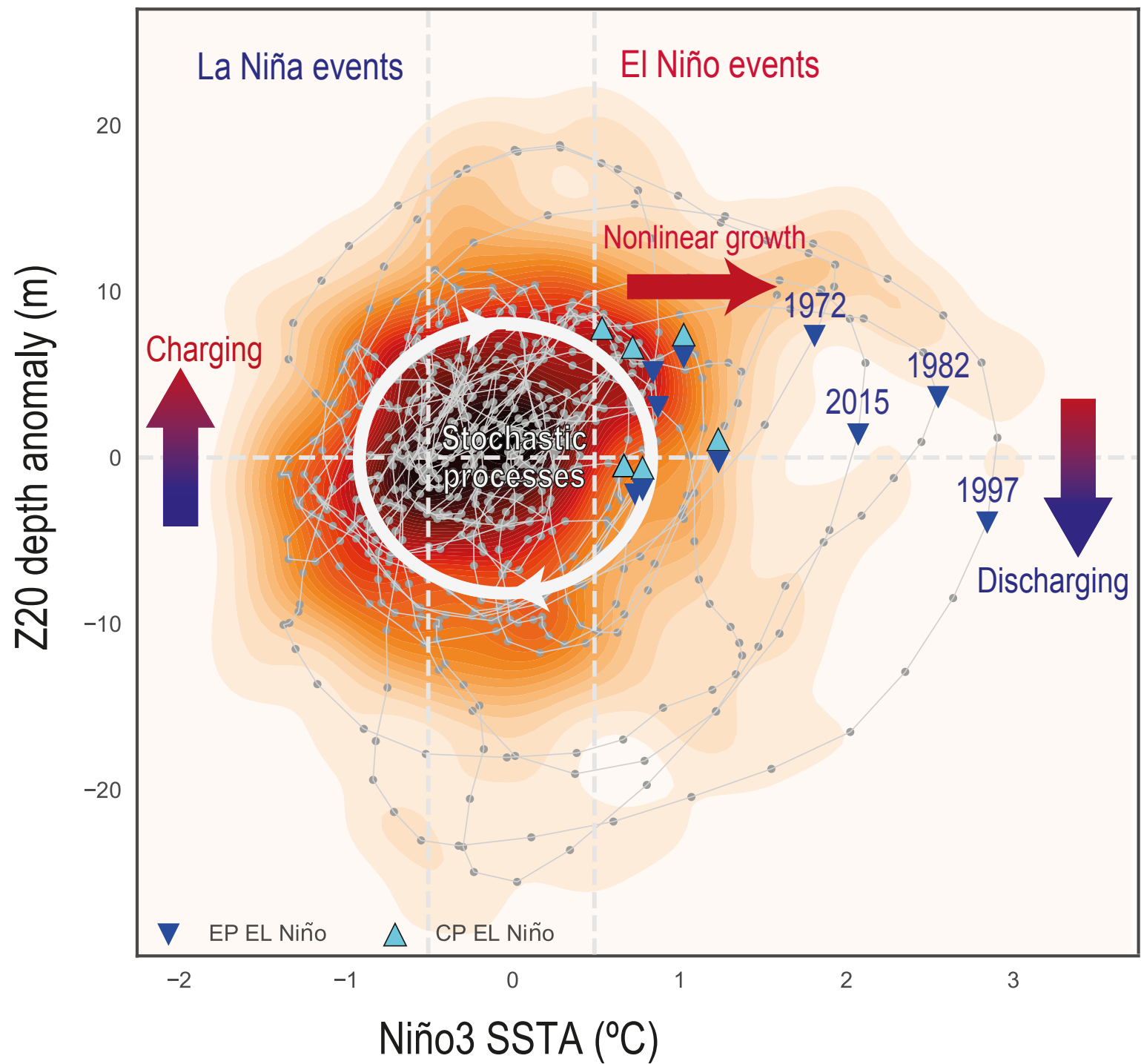
m) 2015/16 EN
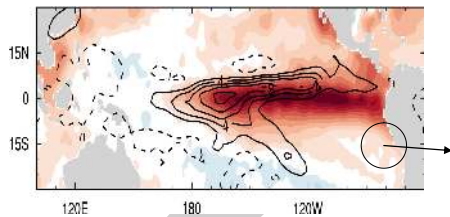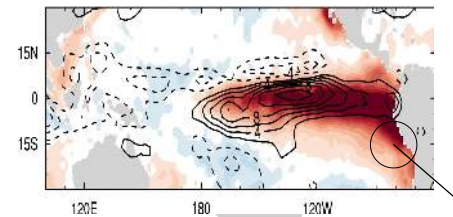
f) 1997/98 EN

l) 2014/15 EN
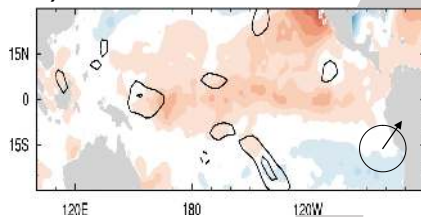
a) 1st EOF pattern (48.92%)
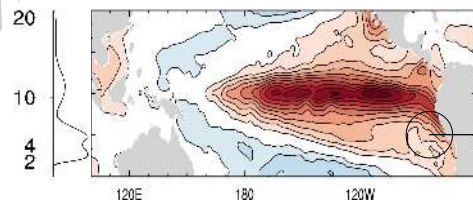
b) 2nd EOF pattern (10.43%)
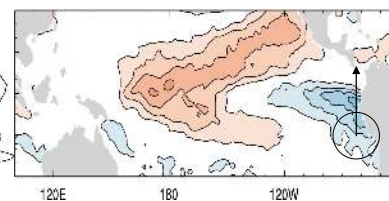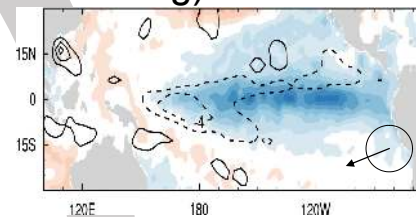
g) 1999/00 LN
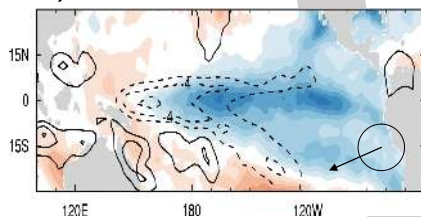
c) 1997-1999
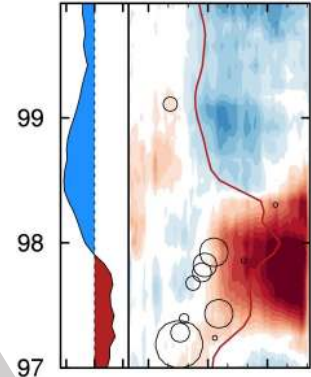
d) 2003-2005

e) 2014-2016

k) 2010/11 LN
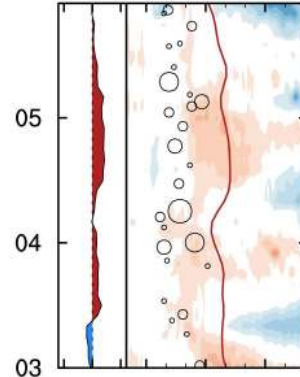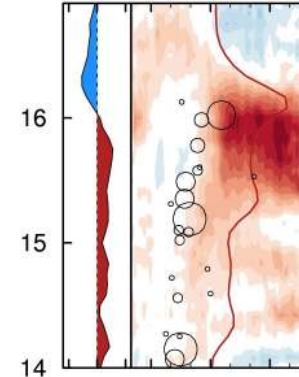
h) 2004/05 EN

j) 2009/10 EN

i) 2006/07 EN

Temperature anomaly (°C)
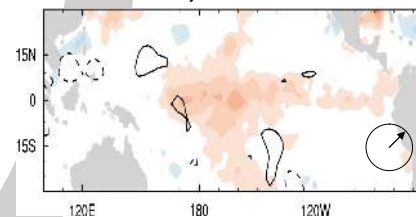
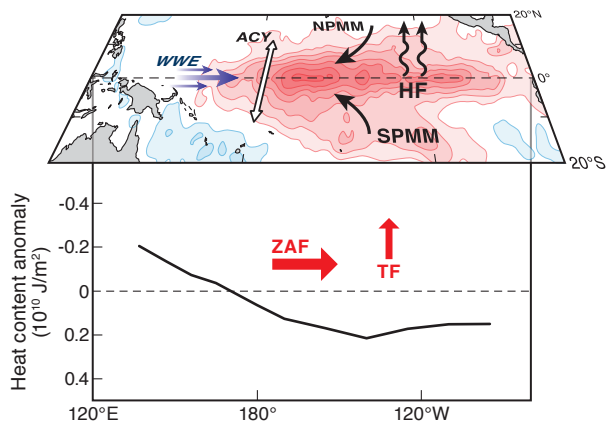QQ Mode

QB Mode
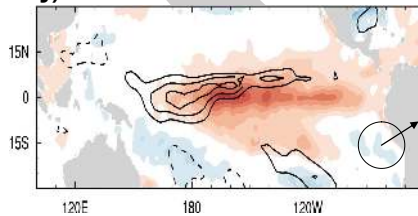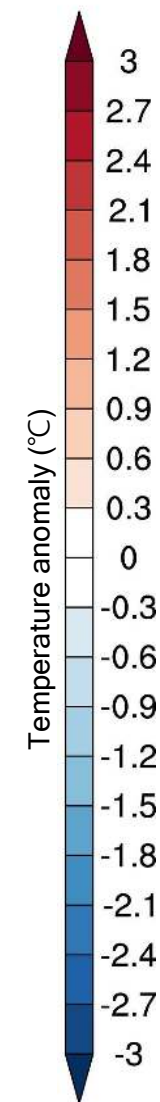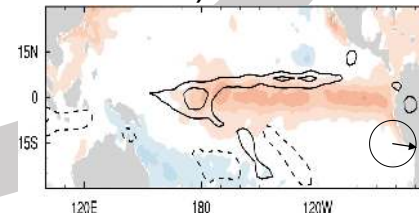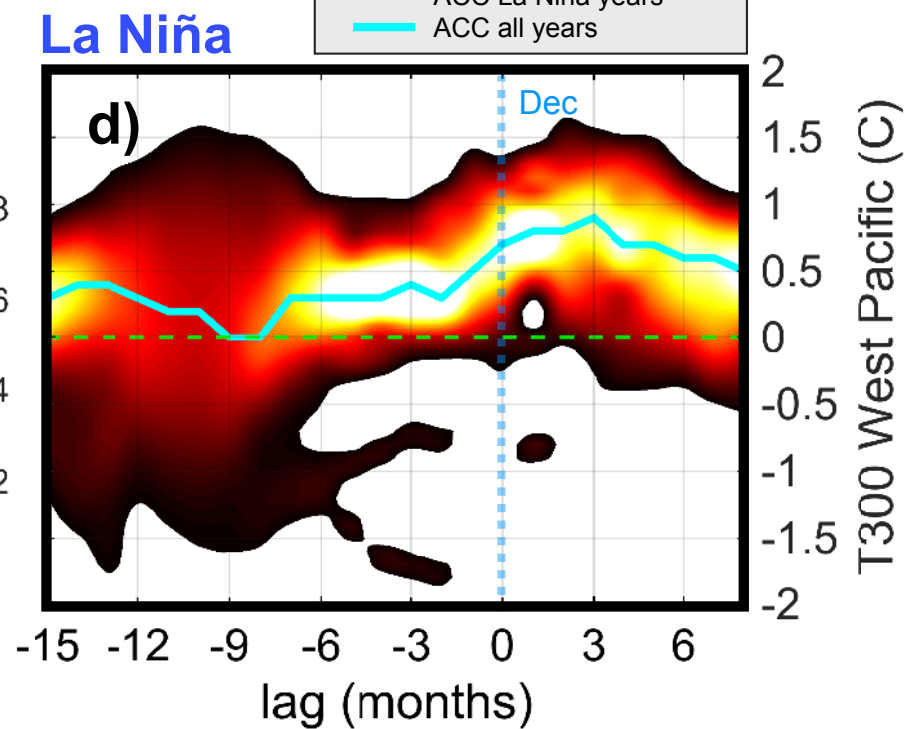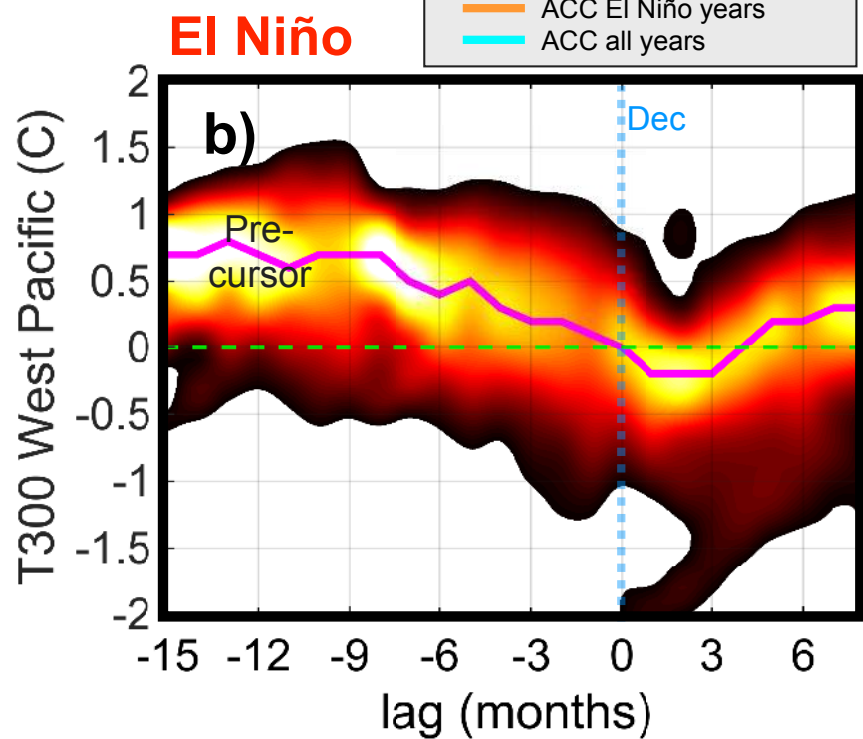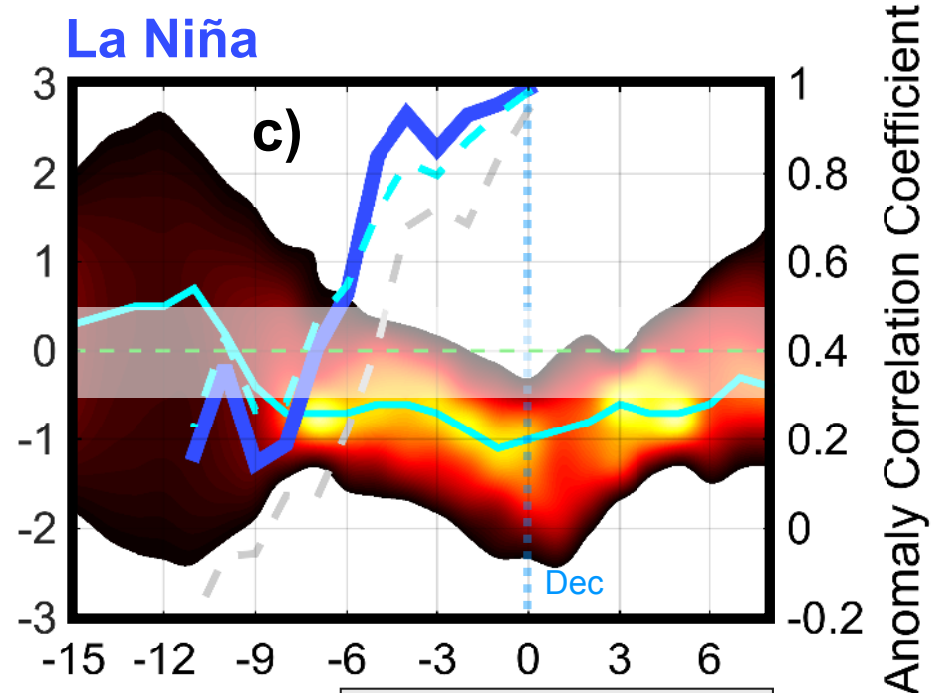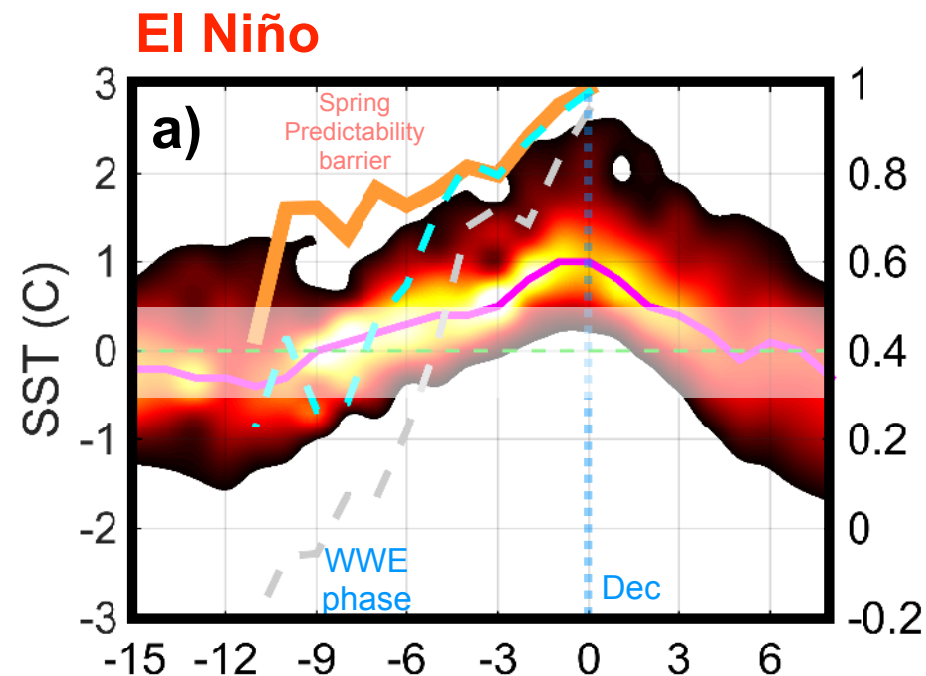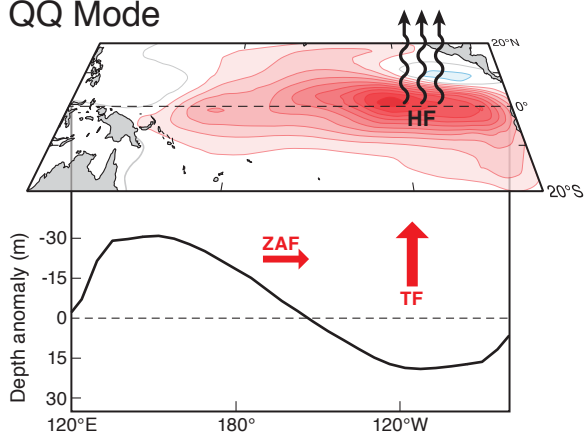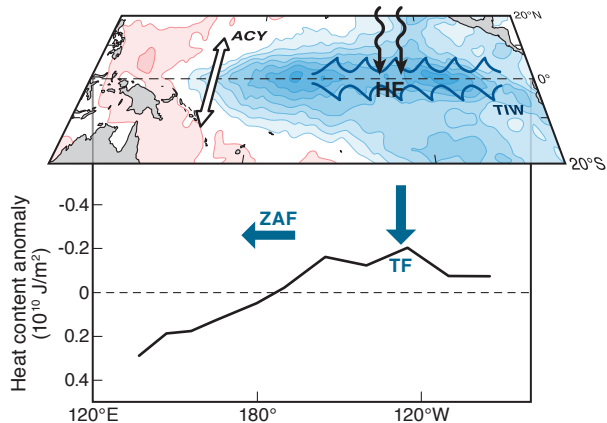
QQ Mode Growth Rate   QB Mode Growth Rate
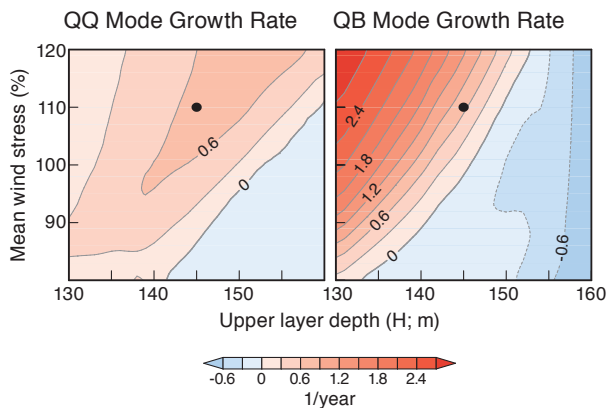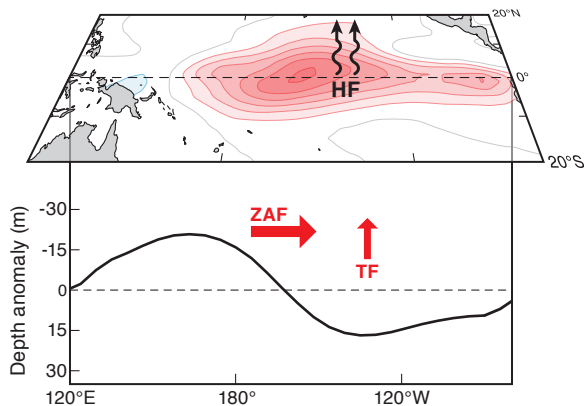
EP 1997/98 **El Niño**
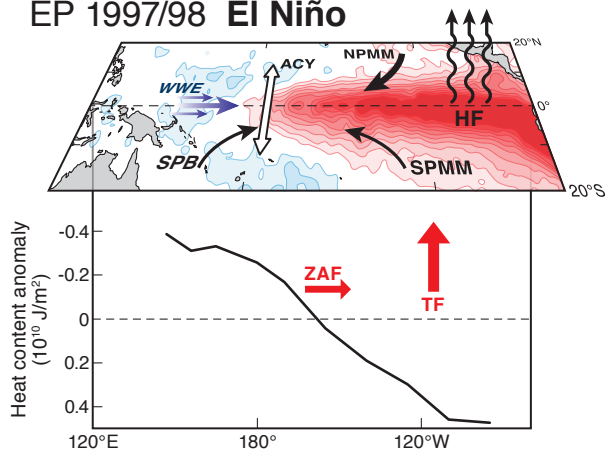
CP 2009 **El Niño**

2010 **La Niña**

Indian Ocean, Atlantic Ocean, and other external forcings